
Differential Uptake of *O*-(2-¹⁸F-Fluoroethyl)-L-Tyrosine, L-³H-Methionine, and ³H-Deoxyglucose in Brain Abscesses

Dagmar Salber^{1,2}, Gabriele Stoffels^{1,2}, Dirk Pauleit^{2,3}, Anna-Maria Oros-Peusquens^{2,3}, Nadim Jon Shah^{2,3}, Peter Klauth⁴, Kurt Hamacher^{2,5}, Heinz Hubert Coenen^{2,5}, and Karl-Josef Langen^{2,3}

¹C. & O. Vogt Institute of Brain Research, Heinrich-Heine-University, Düsseldorf, Germany; ²Brain Imaging Centre West, Research Centre Jülich, Jülich, Germany; ³Institute of Neuroscience and Biophysics–Medicine, Research Centre Jülich, Jülich, Germany; ⁴Institute of Chemistry and Dynamics of the Geosphere, Research Centre Jülich, Jülich, Germany; and ⁵Institute of Neuroscience and Biophysics–Nuclear Chemistry, Research Centre Jülich, Jülich, Germany

The amino acid *O*-(2-¹⁸F-fluoroethyl)-L-tyrosine (¹⁸F-FET) has been shown to be a useful tracer for brain tumor imaging. Experimental studies demonstrated no uptake of ¹⁸F-FET in inflammatory cells but increased uptake has been reported in single cases of human brain abscesses. To explore this inconsistency, we investigated the uptake of ¹⁸F-FET in comparison with that of L-[methyl-³H]methionine (³H-MET) and D-³H-deoxyglucose (³H-DG) in brain and calf abscesses in rats. **Methods:** Abscesses were induced in the brain ($n = 9$) and calf ($n = 5$) of Fisher CDF rats after inoculation of *Staphylococcus aureus*. Five days later, ¹⁸F-FET and ³H-MET ($n = 10$) or ¹⁸F-FET and ³H-DG ($n = 4$) were injected intravenously. One hour after injection the rats were sacrificed, and the brain or calf muscle was investigated using dual-tracer autoradiography. Lesion-to-background ratios (L/B) and standardized uptake values (SUVs) were calculated. The autoradiograms were compared with histology and immunostaining for glial fibrillary acidic protein (GFAP), CD68 for macrophages, and CD11b for microglia. **Results:** ¹⁸F-FET uptake in the area of macrophage infiltration and activated microglia at the rim of the brain abscesses was low (L/B, 1.5 ± 0.4). In contrast, high uptake was observed for ³H-MET as well as for ³H-DG (L/B, 4.1 ± 1.1 for ³H-MET vs. 3.1 ± 1.5 for ³H-DG; $P < 0.01$ vs. ¹⁸F-FET). Results for calf abscesses were similar. In the vicinity of the brain abscesses, slightly increased uptake was noted for ¹⁸F-FET (L/B, 1.8 ± 0.3) and ³H-MET (L/B, 1.8 ± 0.4), whereas ³H-DG distribution was normal (L/B, 1.2 ± 0.2). Anti-GFAP immunofluorescence showed a diffuse astrocytosis in those areas. **Conclusion:** Our results demonstrate that there is no accumulation of ¹⁸F-FET in macrophages and activated microglia in experimental brain abscesses, whereas ³H-MET and ³H-DG exhibit high uptake in these cells. Thus, the specificity of ¹⁸F-FET for gliomas may be superior to that ³H-MET and ³H-DG. Increased ¹⁸F-FET uptake in human brain abscesses appears to be related to reactive astrocytosis.

Key Words: abscess; *O*-(2-¹⁸F-fluoroethyl)-L-tyrosine; L-[methyl-³H]methionine; autoradiography

J Nucl Med 2007; 48:2056–2062
DOI: 10.2967/jnumed.107.046615

The amino acid *O*-(2-¹⁸F-fluoroethyl)-L-tyrosine (¹⁸F-FET) is a powerful PET tracer for the diagnosis of brain tumors, and several studies have demonstrated the clinical potential of this method (1,2). ¹⁸F-FET PET has been shown to be superior to MRI to delineate the solid tumor mass of cerebral gliomas and to differentiate tumor recurrences from unspecific posttherapeutic changes (3,4). In unknown primary lesions, ¹⁸F-FET PET in combination with magnetic resonance spectroscopy was found to have a high predictive value to separate benign from malignant primary lesions (5). Furthermore, a high prognostic value of ¹⁸F-FET PET in combination with MRI was demonstrated in patients with low-grade gliomas (6). In contrast to other amino acid tracers, ¹⁸F-FET can be produced in large amounts and is applicable for PET studies in a satellite concept such as ¹⁸F-FDG (7,8). In contrast to ¹⁸F-FDG and L-[methyl-³H]methionine (³H-MET), animal experiments have shown that ¹⁸F-FET exhibits no uptake in inflammatory cells and in inflammatory lymph nodes, promising a higher specificity for the detection of tumor cells (9,10). However, increased uptake of ¹⁸F-FET in single cases of brain abscesses and in a demyelinating process has been reported recently (11).

Because the acute inflammatory response differs from that of other tissues in the central nervous system (12), animal experiments with ¹⁸F-FET in peripheral abscesses and inflammatory lymph nodes may not have been representative for the specific situation in brain abscesses (9,10). Therefore, there is a need to investigate the specific uptake behavior of ¹⁸F-FET in brain abscesses. Experimental models of brain abscesses have increased our understanding of the neuropathology and the clinical evolution of these lesions

Received Aug. 21, 2007; revision accepted Sep. 6, 2007.
For correspondence or reprints contact: Karl-Josef Langen, MD, Institute of Neuroscience and Biophysics–Medicine, Research Centre Jülich, D-52425 Jülich, Germany.
E-mail: k.j.langen@fz-juelich.de
COPYRIGHT © 2007 by the Society of Nuclear Medicine, Inc.

that parallels the human situation (13). In this study we investigated ^{18}F -FET uptake in rat brain abscesses using dual-tracer autoradiography and immunofluorescent imaging. ^3H -MET and D- ^3H -deoxyglucose (^3H -DG) were chosen as reference tracers and can be considered as the gold standards for brain tumor imaging with PET. Additionally, we compared the uptake of ^{18}F -FET with that of ^3H -MET in some peripheral abscesses as the uptake behavior ^3H -MET in inflammatory lesions is still a matter of discussion.

MATERIALS AND METHODS

Radiopharmaceuticals

The amino acid ^{18}F -FET was produced via phase transfer-mediated nucleophilic ^{18}F -fluorination of *N*-trityl-*O*-(2-tosyloxyethyl)-*L*-tyrosine tert-butylester and subsequent deprotection with a specific radioactivity of >200 GBq/ μmol (8). The uncorrected radiochemical yield was about 35% and radiochemical purity was $>98\%$. The tracer was administered as an isotonic neutral solution.

^3H -MET was obtained commercially with a specific radioactivity of 3 TBq/mmol and ^3H -DG was obtained with a specific radioactivity of 300 GBq/mmol (Amersham Biosciences Europe GmbH).

Animal Experiments

Thirty male Fisher CDF rats (age, 58–94 wk; weight, 180–270 g; Charles River Wiga) were used in this study. The experiments were approved by the district government according to German law on the protection of animals (Cologne/Germany no. 50.203.2-KFA 5/03).

The animals were kept under standard conditions with free access to food and water. Twenty animals were treated to generate brain abscesses and 10 animals were treated to generate calf abscesses according to methods described previously in the literature (13–15). Animals were sedated in an isoflurane atmosphere (2%–5%) and anesthetized with an intraperitoneal injection of ketamine (100 mg/kg)/xylazine (10 mg/kg). For induction of brain abscesses, the animals were placed in a stereotactic frame, the skin covering the skull was incised, and a 0.9-mm burr hole was drilled 2 mm posterior to the bregma and 3 mm lateral to the midline. Using a 50- μL Hamilton syringe, 10 μL of a bacterial suspension (10^7 colony-forming units/mL) (*Staphylococcus aureus*, clinical strain 10B; Novartis Pharma, Inc.) were slowly injected into the brain parenchyma 5 mm from the external surface of the calvarium. Peripheral abscesses were induced by direct injection of 100 μL of the bacterial suspension into the calf muscle.

Five days after injection of the bacteria, animals were reanesthetized for tracer injection. A mixture of 50–100 MBq ^{18}F -FET and 11 MBq ^3H -MET or ^3H -DG was injected via a jugular vein in each animal. The animals were killed 1 h after tracer injection, and the brains or calf muscles were removed immediately and frozen in 2-methylbutane at -50°C . Sections of the abscess-bearing brain and calf muscle were produced (thickness, 20 μm) using a cryostat microtome (CM 3050; Leica Mikrosysteme Vertrieb GmbH).

Autoradiography

The tissue sections were placed on phosphor imaging plates (Raytest-Fuji) along with industrial ^3H activity standards (Microscales; Amersham Biosciences) for ^3H studies and with calibrated ^{18}F liver-paste standards manufactured in-house. The first depiction

of the ^{18}F distribution was started within 2 h after tracer injection, with a duration of 14 h. This exposition was done on imaging plates insensitive to β^- -particles of ^3H (BAS-SR 2025; Raytest-Fuji). After decay of ^{18}F (10 half-lives), the brain slices were exposed to ^3H -sensitive imaging plates for 72 h to obtain the ^3H distribution (BAS-TR 2025; Raytest-Fuji). On exposure, the imaging plates were scanned with a high-performance imaging plate reader (BAS 5000 BioImage Analyzer; Raytest-Fuji). Quantitative autoradiograms were generated (Bq/mg wet weight of the tissue) using the software provided by the manufacturer and the known radioactivity concentrations of the standards. The autoradiograms were evaluated by circular regions of interest (ROIs) placed on areas with maximal tracer uptake at the rim of the abscesses (size, 0.7 ± 0.4 mm 2) and the contralateral normal brain tissue or unaffected muscle (size, 2 mm 2). In brain abscesses, additional ROIs were placed in the vicinity of the abscesses, which showed slightly increased ^{18}F -FET and ^3H -MET uptake. These areas exhibited a normal cell structure on histologic staining using toluidine blue. However, immunofluorescent imaging showed a diffuse astrocytosis. Standardized uptake values (SUVs) were calculated by normalization of the average uptake (Bq/mg) in the ROIs of maximal tracer uptake in the lesion (SUV $_{\text{max}}$) versus the average uptake in the contralateral gray matter or normal muscle tissue (background) to the injected dose and body weight. Lesion-to-background ratios (L/B) were calculated by dividing the SUV $_{\text{max}}$ in the lesion by the SUV in the normal tissue.

Double Immunofluorescent Labeling and Histologic Staining

Double immunofluorescent labeling was performed on serial slices to identify specific subtypes of cells involved in the process of tracer uptake. Macrophages were demonstrated with mouse antirat CD68 monoclonal antibodies (1:50; Serotec). Reactive astrocytes in brain slices were detected by staining for glial fibrillary acidic protein (GFAP) using rabbit antirat GFAP polyclonal antibodies (1:1,000; abcam) and microglia with mouse antirat CD11b monoclonal antibodies (1:50; AbD Serotec). As the secondary antibody, goat antirabbit Alexa Fluor 568 or goat antimouse Alexa Fluor 488 (1:300; Invitrogen) was used. Tissue slices were counterstained with 4',6'-diamidino-2-phenylindole hydrochloride (DAPI; 2 $\mu\text{g}/\text{mL}$), which is known to form fluorescent complexes with natural double-stranded DNA (Sigma-Aldrich Chemie GmbH). In addition, tissue slices were histologically stained by toluidine blue or hematoxylin in serial slices.

MRI

To compare the distribution of ^{18}F -FET and ^3H -MET with conventional MRI and blood-brain barrier (BBB) disruption as determined by contrast enhancement after injection of the paramagnetic contrast agent gadolinium diethylenetriaminepentaacetic acid (Gd-DTPA [Magnevist]; Schering), 10 animals were also investigated by MRI before ^{18}F -FET and ^3H -MET injection. MR examinations were performed with a 9.4-T animal scanner. The scanner was based on a superconducting magnet (Magnex) with a 16-cm bore size, equipped with a 10-cm inner-diameter gradient coil (Magnex), capable of a maximum gradient strength of 270 mT/m/axis and a Varian Unity Inova console. A surface coil of 3-cm diameter was used for both radiofrequency (RF) transmission and signal reception. The animals were anesthetized by injection of ketamine as described before the MR scan and were positioned in an acrylic holder equipped with a bite bar and ear restraints. The RF coil was placed in a fixed geometry immediately

TABLE 1
Data on Animals with Brain Abscesses

No.	¹⁸ F-FET uptake in abscess wall and vicinity				³ H-MET uptake in abscess wall and vicinity				³ H-DG uptake in abscess wall and vicinity			
	SUVmax abscess	SUV vicinity	L/B abscess	L/B vicinity	SUVmax abscess	SUV vicinity	L/B abscess	L/B vicinity	SUVmax abscess	SUV vicinity	L/B abscess	L/B vicinity
1	1.3	1.6	1.9	2.2	6.1	3.7	4.1	2.5				
2	1.1	1.4	1.5	1.9	2.3	1.0	3.3	1.4				
3	1.1	1.5	1.3	1.7	4.2	2.8	2.7	1.8				
4	1.8	1.8	2.1	2.2	7.7	2.6	5.5	1.9				
5	1.6	1.4	1.5	1.7	8.5	2.7	4.9	1.6				
6	0.5	0.6	1.7	2.2					7.4	2.5	2.8	1.5
7	2.1	1.5	1.1	1.4					10.3	4.4	2.1	1.0
8	1.9	3.0	1.0	1.5					18.5	8.6	2.3	1.1
9	1.6	2.1	1.4	1.8					15.1	2.8	5.3	1.0
Mean	1.4	1.7	1.5	1.8*	5.8†	2.6	4.1†	1.8*	12.8†	4.6	3.1†	1.2
SD	0.5	0.6	0.4	0.3	2.5	1.0	1.1	0.4	4.9	2.8	1.5	0.2

**P* < 0.01 vs. ³H-DG.
†*P* < 0.01 vs. ¹⁸F-FET.

above the skull of the animal. A catheter was inserted in the tail vein, allowing for contrast agent to be injected without changing the position of the animal inside the scanner. During the MR examination, the body temperature of the rat was maintained constant by use of a heating pad. A T1-weighted protocol was used before and 2 min after injection of 150 μL Gd-DTPA. The measurement parameters for the spin-echo sequence included repetition time, 1,000 ms; echo time, 10.5 ms; field of view, 30 × 30 mm; and matrix size, 256 × 256, close to whole-brain coverage using 2 sets of 16 slices of 0.5-mm thickness and 0.5-mm gap, 3 averages. The total acquisition time of the MR protocol, before and after contrast, was approximately 50 min.

Statistical Analysis

Values are expressed as mean ± SD. Statistical methods used were the *t* test or the Mann–Whitney rank sum test for group comparisons, 1-way ANOVA using the Student–Newman–Keuls method for multiple comparison, or the Kruskal–Wallis 1-way ANOVA on ranks using the Dunn method. Probability values < 0.05 were considered significant.

RESULTS

Purulent brain abscesses developed in 9 of 20 animals and calf abscesses developed in 5 of 10 animals. The animals with manifest disease were in a poor condition and suffered from weight loss, so the autoradiographic experiments were performed no later than 5 d after inoculation of the bacteria. Only the animals with purulent abscesses were considered for further evaluation. ¹⁸F-FET uptake in the area of macrophage infiltration and microglial activation at the rim of the brain abscesses as indicated by anti-CD68 and anti-CD11b immunofluorescence was low (SUV_{max}, 1.4 ± 0.5; L/B, 1.5 ± 0.4; *n* = 9) (Table 1; Fig. 1). In contrast, high uptake in the area of macrophage infiltration was observed for ³H-MET (SUV_{max}, 5.8 ± 2.5; L/B, 4.1 ± 1.1; *n* = 5; *P* < 0.01 vs. ¹⁸F-FET) as well as for ³H-DG (SUV_{max}, 12.8 ± 4.9; L/B, 3.1 ±

1.5; *n* = 4; *P* < 0.01 vs. ¹⁸F-FET). MRI after injection of contrast medium showed a typical ring enhancement in that area indicating BBB disruption. In the vicinity of the brain abscesses, moderately increased uptake was noted for ¹⁸F-FET (SUV_{max}, 1.7 ± 0.6; L/B, 1.8 ± 0.3; *n* = 9) and ³H-MET (SUV_{max}, 2.6 ± 1.0; L/B, 1.8 ± 0.4; *n* = 5), whereas ³H-DG distribution was similar to that of normal brain (SUV_{max}, 4.6 ± 2.8; L/B, 1.2 ± 0.2; *n* = 4; *P* < 0.01 vs. ¹⁸F-FET and ³H-MET). Anti-GFAP immunofluorescence showed a diffuse astrocytosis in those areas. Examples of ¹⁸F-FET uptake and ³H-MET or ³H-DG uptake in cerebral abscesses in comparison with immunofluorescent staining or MRI are shown in

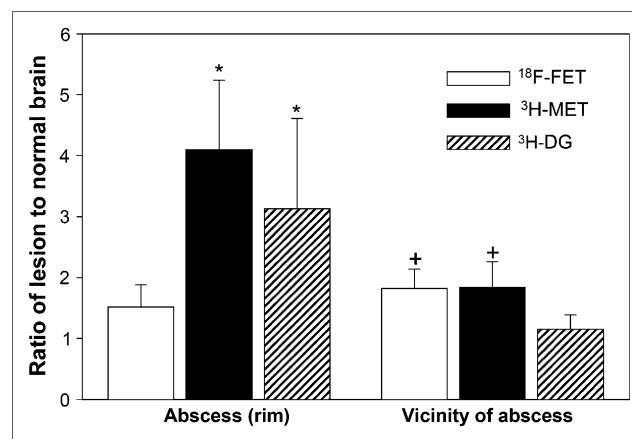


FIGURE 1. Comparison of lesion-to-normal brain ratios of ¹⁸F-FET, ³H-MET, and ³H-DG. (Left) Data for abscess rim (macrophage infiltration). (Right) Data for vicinity of abscess. Uptake of ³H-MET and ³H-DG is significantly increased in macrophages (**P* < 0.01 vs. ¹⁸F-FET), whereas uptake of ¹⁸F-FET is close to that in normal brain tissue. In vicinity of abscess, slightly increased uptake of ¹⁸F-FET and ³H-MET is noted (†*P* < 0.01 vs. ³H-DG), whereas ³H-DG uptake is unchanged.

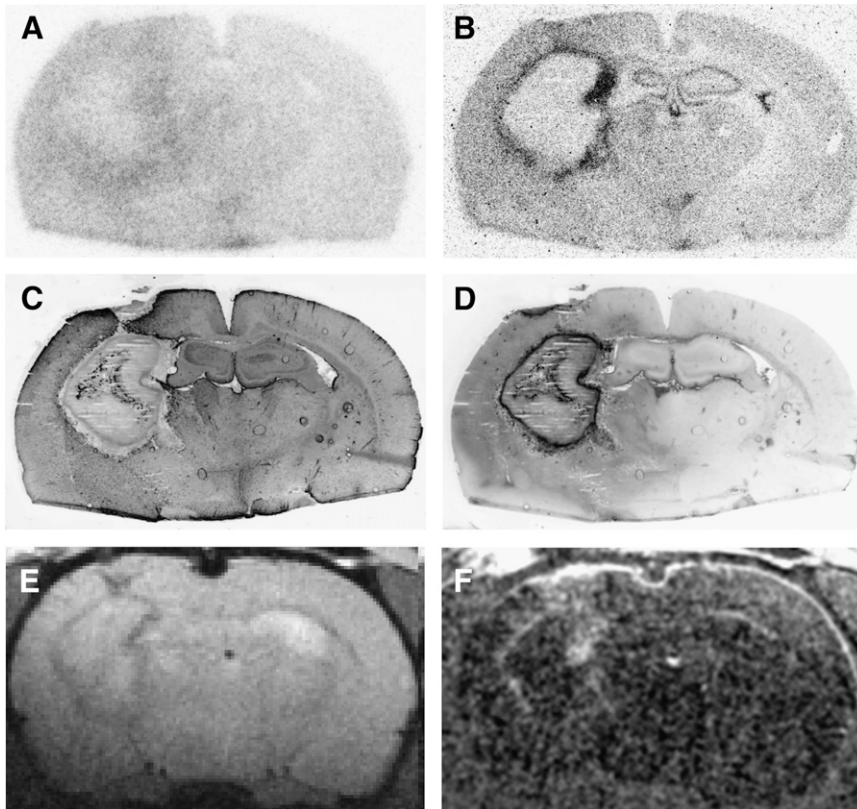


FIGURE 2. Coronal rat brain slices 5 d after abscess induction (rat 4). (A) ^{18}F -FET autoradiography. (B) ^3H -MET autoradiography. (C) Immunofluorescent imaging for GFAP. (D) Immunofluorescent imaging for CD68. (E) T1-weighted MRI. (F) Contrast-enhanced T1-weighted MRI after intravenous injection of Gd-DTPA (subtraction). Increased ^3H -MET uptake in abscess rim is congruent with macrophage infiltration. ^{18}F -FET is negative in that area. MRI shows typical ring-enhancing lesion.

Figures 2, 3, and 4. Results in peripheral abscesses were similar. ^{18}F -FET uptake in the area of macrophage infiltration at the rim of the calf abscesses was low (SUV_{max} , 1.7 ± 0.2 ; L/B, 1.0 ± 0.1 ; $n = 5$) (Table 2). In contrast, high uptake in macrophages was observed for ^3H -MET (SUV_{max} , 6.5 ± 2.2 ; L/B, 4.2 ± 0.6 ; $n = 5$; $P < 0.01$ vs. ^{18}F -FET). An example is shown in Figure 5 (animal 11).

DISCUSSION

The purpose of this study was to investigate the specific uptake behavior of ^{18}F -FET in brain abscesses. Several studies have shown that the uptake of ^{18}F -FET in macro-

phages and inflammatory lesions is low and that the tracer is better suited to differentiate between tumor and inflammation than ^{18}F -FDG or ^{11}C -MET. This has been demonstrated in animal experiments with peripheral abscesses (9) and inflammatory lymph nodes (10), in inflammatory cells in vitro (15), and in patients with head and neck tumors (16).

Recently, however, we observed high ^{18}F -FET uptake in 2 of 6 human brain abscesses and a demyelinating lesion (11). This observation raised the question of whether the uptake behavior of ^{18}F -FET in inflammatory lesions in the brain may be different from that in inflammatory lesions in other tissues.

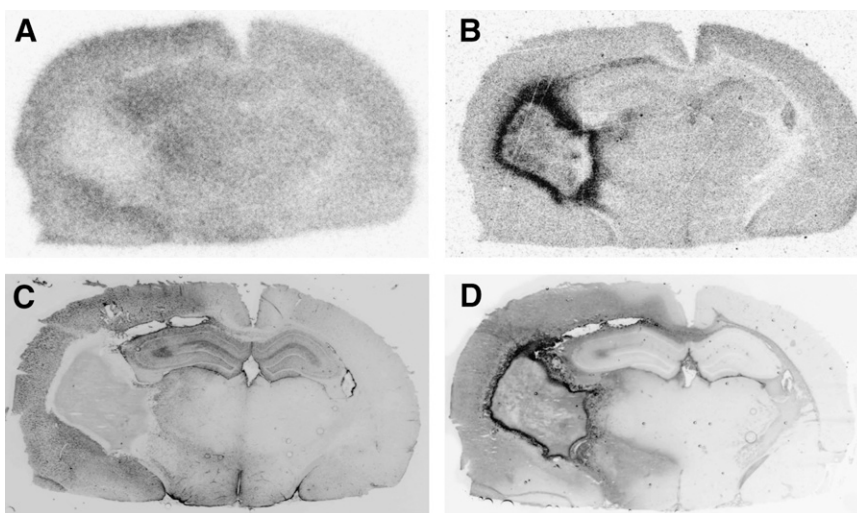


FIGURE 3. Coronal rat brain slices 5 d after abscess induction (rat 9). (A) ^{18}F -FET autoradiography. (B) ^3H -DG autoradiography. (C) Immunofluorescent imaging for GFAP. (D) Immunofluorescent imaging for CD68. Increased ^3H -DG uptake in abscess rim is congruent with macrophage infiltration. Again, ^{18}F -FET is negative in that area. However, diffuse ^{18}F -FET uptake in vicinity of abscess shows similarity to reactive astrocytosis (GFAP).

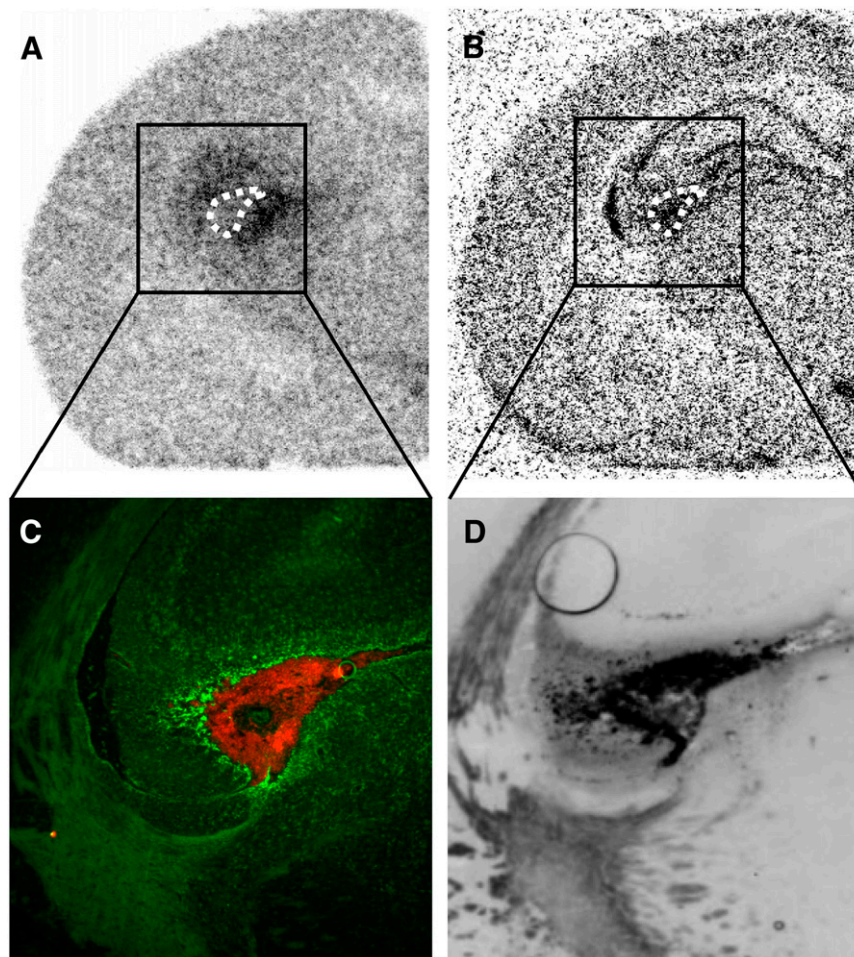


FIGURE 4. Coronal rat brain slices 5 d after abscess induction (rat 1). (A) ^{18}F -FET autoradiography. (B) ^3H -MET autoradiography. (C) Overlay of double immunofluorescent imaging for astrocytosis (GFAP, green) and microglia (CD11b, red). (D) Immunofluorescent imaging for CD68. C and D are same area at higher magnification. Dotted line indicates position of area with increased GFAP and CD68 binding in autoradiograms. Increased ^{18}F -FET uptake appears to be colocalized with reactive astrocytosis in surrounding of this area (green cells), whereas increased ^3H -MET uptake is found in area of activated microglia (red cells) that also shows immunoreactivity for macrophages (D).

Indeed, it is well known that the acute inflammatory response in the central nervous system differs from that of other tissues (12). In peripheral tissues, circulating neutrophils and monocytes, which are the precursors of macrophages, are delivered to the site of infection. The phagocytes then function at the site of injury to kill invading microorganisms, remove debris, and facilitate tissue repair. In the brain, the presence of the BBB largely excludes neutrophil migration and plasma components that contribute to inflam-

matory reaction and there are no mast cells to release stored proinflammatory molecules (12). Instead, microglia, the resident macrophages of the nervous system, become activated and synthesize proinflammatory molecules and chemoattractants. This is followed by proliferation and hypertrophy of astrocytes.

The rat brain model closely mimics human disease in that the abscess progresses through a series of well-defined stages (13). Each stage is defined on the basis of predominant cell

TABLE 2
Data on Animals with Calf Abscesses

No.	^{18}F -FET uptake in abscess wall			^3H -MET uptake in abscess wall		
	SUVmax abscess	SUV muscle	L/B abscess	SUVmax abscess	SUV muscle	L/B abscess
10	1.7	1.6	1.1	5.1	1.3	4.0
11	1.7	1.5	1.1	6.7	1.7	4.6
12	1.5	1.5	1.0	9.3	2.0	4.6
13	1.9	2.1	0.9	7.9	1.7	4.6
14	1.5	1.8	0.9	3.7	1.2	3.2
Mean	1.7	1.7	1.0	6.5	1.6	4.2*
SD	0.2	0.3	0.1	2.2	0.3	0.6

* $P < 0.01$ vs. L/B of FET.

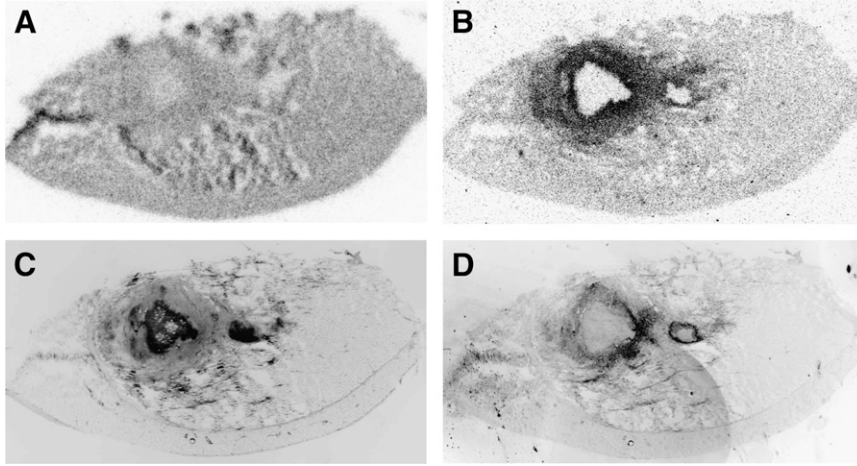


FIGURE 5. Slices of calf muscle 5 d after abscess induction (rat 11). (A) ^{18}F -FET autoradiography. (B) ^3H -MET autoradiography. (C) Immunofluorescent imaging for cell nuclei (DAPI). (D) Immunofluorescent imaging for macrophages (CD68). Increased ^3H -MET uptake in abscess rim is congruent with macrophage infiltration. ^{18}F -FET is negative in that area.

types and the histologic appearance of the abscess. In humans, these stages have been identified using CT (17). The early stage, or early cerebritis, occurs from days 1 to 3 and is typified by diffuse microglial activation and diffuse astrocytosis, tissue necrosis, and edema. The intermediate, or late cerebritis, stage occurs from days 4 to 9 and is associated with a predominant macrophage and lymphocyte infiltrate. At this stage, the determination of the origin of the phagocytes is difficult because microglia, the resident macrophages of the brain, become indistinguishable from hematogenous macrophages on morphologic grounds and based on the expression of immunocytochemical markers after activation (18). In the final, or capsule, stage from day 10 onward, the microglial and astrocytic responses become restricted to the area around the lesion and are associated with the formation of a well-vascularized abscess wall.

The experiments in the present study were performed in the stage of late cerebritis at 5 d after inoculation of bacteria. This time point was chosen because at this stage macrophages and reactive astrocytosis are not yet colocalized to the area around the lesion, and an allocation of tracer uptake to specific cell types is feasible. MRI displayed a typical ring enhancement in the abscess area, indicating BBB disruption. We found no uptake of ^{18}F -FET in the area of macrophage infiltration and microglial activation at the rim of the brain abscesses, whereas the uptake of ^3H -MET and ^3H -DG was clearly positive in these cells. Thus, it can be concluded that there is no uptake of ^{18}F -FET by macrophages or activated microglia. Furthermore, the results demonstrate that BBB disruption does not necessarily induce increased FET uptake.

However, diffuse uptake of ^{18}F -FET was found in the vicinity of brain abscesses that showed a similarity to the area of reactive astrocytosis as demonstrated by GFAP staining. A diffuse reactive astrocytosis throughout the injected hemisphere is typical in the abscess model at day 5–6 after induction (13). In a recent study, we investigated the differential uptake behavior of ^{18}F -FET and ^3H -MET in focal cortical infarctions (19). In that study, we identified some lesions with an incongruity of ^{18}F -FET and ^3H -MET uptake

in the infarct area, and immunofluorescent imaging revealed that selective uptake of ^{18}F -FET was associated with GFAP-positive astroglia, whereas selective ^3H -MET uptake correlated with CD68-positive macrophage infiltration. Therefore, the finding of similarity between diffuse astrocytosis and diffusely increased FET uptake supports the hypothesis of a specific affinity of ^{18}F -FET for reactive astrocytosis.

It is tempting to speculate that the accumulation ^{18}F -FET uptake in human brain abscesses and demyelinating lesions is due to increased uptake in reactive astrocytosis. Human brain abscesses and the demyelinating process in our previous study were known for >8 d, so that a final or capsule stage was present (11). Both brain abscesses and demyelinating lesions may be accompanied by marked reactive gliosis; therefore, increased uptake of ^{18}F -FET in these cases might have been caused by uptake in those cells. Also, an experimental study in acute cerebral radiation injury observed increased ^{18}F -FET uptake in the inflammatory layer around the radiation necrosis, which was characterized by a dense infiltrate of macrophages and reactive astrocytosis (20).

Furthermore, our experiments demonstrated no uptake of ^{18}F -FET in macrophages in peripheral abscesses, which confirms the results of previous studies (9). Additionally, we showed that ^3H -MET is clearly positive in the area of macrophage infiltration at the rim of the calf abscesses, indicating a poor specificity of ^{11}C -MET to differentiate between tumors and inflammation. This is in contrast to other experimental studies that reported uptake of ^{14}C -MET predominantly in viable tumor cells, with low uptake in macrophages and other cells (21). Our observations, however, are in line with case reports and studies on small patient groups that have shown accumulation of ^{11}C -MET in brain abscesses (22–24).

It must be considered that the discordant uptake of ^{18}F -FET and ^3H -MET in macrophages indicates differences in the uptake mechanisms of the 2 amino acids. Experimental studies suggest that the transport mechanisms of ^{18}F -FET and ^3H -MET in glioma cells in vitro were comparable in

principle (25,26). Recent studies in patients with peripheral tumors, however, found no uptake of ^{18}F -FET in most peripheral tumors, especially in lymphomas and most adenocarcinomas, which is in contrast to the results obtained with ^{11}C -MET and different tyrosine derivatives (27). It was speculated that ^{18}F -FET may be transported via a specific subtype of the system L-amino acid transporter that is not ubiquitously expressed.

CONCLUSION

Our results in experimental brain abscesses demonstrate that there is no accumulation of ^{18}F -FET in macrophages and activated microglia, whereas ^3H -MET and ^3H -DG exhibit high uptake in these cells. Thus, the specificity of ^{18}F -FET for gliomas may be superior to that ^3H -MET and ^3H -DG. Increased ^{18}F -FET uptake in human brain abscesses appears to be related to reactive astrocytosis.

ACKNOWLEDGMENTS

The authors thank Stephanie Klein for technical assistance, Norbert Hartwigsen for animal husbandry, and Erika Wabbals, Silke Grafmüller, and Sascha Rehbein for technical assistance in radiosynthesis of ^{18}F -FET. This work was supported by the Deutsche Forschungsgemeinschaft (grant La-1263/1-3) and by the Brain Imaging Centre West. The facility for magnetic resonance imaging at the Institute of Medicine, Research Centre Jülich, was supported by the Bundesministerium für Bildung und Forschung grant BMBF 01GO0104.

REFERENCES

- Langen KJ, Hamacher K, Weckesser M, et al. O-(2-[^{18}F]Fluoroethyl)-L-tyrosine: uptake mechanisms and clinical applications. *Nucl Med Biol.* 2006;33:287–294.
- Weckesser M, Langen KJ, Rickert CH, et al. O-(2-[^{18}F]Fluoroethyl)-L-tyrosine PET in the clinical evaluation of primary brain tumors. *Eur J Nucl Med Mol Imaging.* 2005;32:422–429.
- Pauleit D, Floeth F, Hamacher K, et al. O-(2-[^{18}F]Fluoroethyl)-L-tyrosine PET combined with MRI improves the diagnostic assessment of cerebral gliomas. *Brain.* 2005;128:678–687.
- Pöppel G, Gotz C, Rachinger W, et al. Value of O-(2-[^{18}F]fluoroethyl)-L-tyrosine PET for the diagnosis of recurrent glioma. *Eur J Nucl Med Mol Imaging.* 2004;31:1464–1470.
- Floeth FW, Pauleit D, Wittsack HJ, et al. Multimodal metabolic imaging of cerebral gliomas: positron emission tomography with [^{18}F]fluoroethyl-L-tyrosine and magnetic resonance spectroscopy. *J Neurosurg.* 2005;102:318–327.
- Floeth FW, Pauleit D, Sabel M, et al. Prognostic value of O-(2-[^{18}F]fluoroethyl)-L-tyrosine PET and MRI in low-grade glioma patients. *J Nucl Med.* 2007;48:519–527.
- Wester HJ, Herz M, Weber W, et al. Synthesis and radiopharmacology of O-(2-[^{18}F]fluoroethyl)-L-tyrosine for tumor imaging. *J Nucl Med.* 1999;40:205–212.
- Hamacher K, Coenen HH. Efficient routine production of the ^{18}F -labelled amino acid O-(2-[^{18}F]fluoroethyl)-L-tyrosine. *Appl Radiat Isot.* 2002;57:853–856.
- Kaim AH, Weber B, Kurrer MO, et al. ^{18}F -FDG and ^{18}F -FET uptake in experimental soft tissue infection. *Eur J Nucl Med Mol Imaging.* 2002;29:648–654.
- Rau FC, Weber WA, Wester HJ, et al. O-(2-[^{18}F]Fluoroethyl)-L-tyrosine (^{18}F -FET): a tracer for differentiation of tumour from inflammation in murine lymph nodes. *Eur J Nucl Med Mol Imaging.* 2002;29:1039–1046.
- Floeth FW, Pauleit D, Sabel M, et al. ^{18}F -FET PET differentiation of ring enhancing brain lesions. *J Nucl Med.* 2006;47:776–782.
- Perry VH, Andersson PB, Gordon S. Macrophages and inflammation in the central nervous system. *Trends Neurosci.* 1993;16:268–273.
- Flaris NA, Hickey WF. Development and characterization of an experimental model of brain abscess in the rat. *Am J Pathol.* 1992;141:1299–1307.
- Winn HR, Mendes M, Moore P, Wheeler C, Rodeheaver G. Production of experimental brain abscess in the rat. *J Neurosurg.* 1979;51:685–690.
- Stober B, Tanase U, Herz M, et al. Differentiation of tumour and inflammation: characterisation of [methyl- ^3H]methionine (MET) and O-(2-[^{18}F]fluoroethyl)-L-tyrosine (FET) uptake in human tumour and inflammatory cells. *Eur J Nucl Med Mol Imaging.* 2006;33:932–939.
- Pauleit D, Zimmermann A, Stoffels S, et al. ^{18}F -FET PET compared with ^{18}F -FDG PET in patients with head and neck cancer. *J Nucl Med.* 2006;47:256–261.
- Britt RH, Enzmann DR, Yeager AS. Neuropathological and computerized tomographic findings in experimental brain abscess. *J Neurosurg.* 1981;55:590–603.
- Stoll G, Jander S, Schroeter M. Inflammation and glial responses in ischemic brain lesions. *Prog Neurobiol.* 1998;56:149–171.
- Salber D, Stoffels G, Pauleit D, et al. Differential uptake of ^{18}F -FET and ^3H -L-methionine in focal cortical ischemia. *Nucl Med Biol.* 2006;33:1029–1035.
- Spaeth N, Wyss MT, Weber B, et al. Uptake of ^{18}F -fluorocholeline, ^{18}F -fluoroethyl-L-tyrosine, and ^{18}F -FDG in acute cerebral radiation injury in the rat: implications for separation of radiation necrosis from tumor recurrence. *J Nucl Med.* 2004;45:1931–1938.
- Kubota R, Kubota K, Yamada S, et al. Methionine uptake by tumor tissue: a microautoradiographic comparison with FDG. *J Nucl Med.* 1995;36:484–492.
- Ishii K, Ogawa T, Hatazawa J, et al. High L-methyl-[^{11}C]methionine uptake in brain abscess: a PET study. *J Comput Assist Tomogr.* 1993;17:660–661.
- Mineura K, Sasajima T, Kowada M, et al. Indications for differential diagnosis of nontumor central nervous system diseases from tumors: a positron emission tomography study. *J Neuroimaging.* 1997;7:8–15.
- Tsuyuguchi N, Sunada I, Ohata K, et al. Evaluation of treatment effects in brain abscess with positron emission tomography: comparison of fluorine-18-fluorodeoxyglucose and carbon-11-methionine. *Ann Nucl Med.* 2003;17:47–51.
- Langen KJ, Jarosch M, Mühlensiepen H, et al. Comparison of fluoro-tyrosines and methionine uptake in F98 rat gliomas. *Nucl Med Biol.* 2003;30:501–508.
- Weber WA, Wester HJ, Grou AL, et al. O-(2-[^{18}F]Fluoroethyl)-L-tyrosine and L-[methyl- ^{11}C]methionine uptake in brain tumours: initial results of a comparative study. *Eur J Nucl Med.* 2000;27:542–549.
- Pauleit D, Stoffels G, Schaden W, et al. PET with O-(2-[^{18}F]fluoroethyl)-L-tyrosine (^{18}F -FET) in peripheral tumours: first clinical results. *J Nucl Med.* 2005;46:411–416.